An ingestible device for gastric electrophysiology

Siheng Sean You[1,2,7], Adam Gierlach[1,3,7], Paul Schmidt [1,2,4], George Selsing[1,2], Injoo Moon[1,2], Keiko Ishida[1,2], Josh Jenkins [1,5], Wiam A. M. Madani[1,2], So-Yoon Yang[1,3], Hen-Wei Huang [1,2,5], Stephanie Owyang [1,2], Alison Hayward[1,2,6], Anantha P. Chandrakasan [3] & Giovanni Traverso [1,2,5] ✉

The ability to record high-quality electrophysiology data from the gastrointestinal tract and enteric nervous system is of use in understanding a variety of disorders and improving healthcare via early diagnosis. However, such measurements remain challenging because electrodes must be implanted surgically or worn on the skin, which results in a trade-off between signal quality and invasiveness. Here we report an ingestible device for gastric electrophysiology. The non-invasive system, which is termed multimodal electrophysiology via ingestible, gastric, untethered tracking (MiGUT), consists of encapsulated electronics and a sensing electrode ribbon that unrolls in the stomach following delivery to make contact with the mucosa. The device then records and wirelessly transmits biopotential signals to an external receiver. We show that the device can record electrical signals—including the gastric slow wave, respiration signal and heart signal—in a large animal model and can monitor slow wave activity in freely moving and feeding animals.

The enteric nervous system (ENS) contains millions of neurons and associated electrically active cells that regulate motility and hormone secretion in the gastrointestinal (GI) tract[1,2]. Dysfunction in electrical signalling is associated with a wide range of debilitating GI disorders. These include gastroparesis, which can arise either idiopathically or as a complication of diabetes[3,4] and functional dyspepsia, which has an estimated worldwide prevalence of 10–30% (ref. 5). There is also mounting evidence of a gut–brain axis dysfunction in many neurological disorders; patients who develop Parkinson's are reported to exhibit early GI motility issues[6–8] and gastrointestinal issues are widespread in those with autism spectrum disorder[9,10]. Monitoring of baseline GI electrophysiology is limited[11–13], which makes it difficult to differentiate changes due to regular daily activities from those arising from disease pathology. Consequently, methods that can interrogate the electrical

signalling of the ENS throughout the GI tract with high fidelity could advance fundamental understanding of these disorders and improve healthcare via differential or early disease diagnosis.

Effectively capturing GI biopotentials is difficult due to the depth of the signals' origin within the GI tract. In the context of the stomach, with its 3–4 cycles per min gastric slow wave[14], cutaneous electrogastrography was discovered in the early 20th century[15] but was not widely adopted due to attenuation of the signal through the abdominal tissue and artefacts arising from motion or myoelectric activity[11,12]. High resolution mapping via serosal surgical placement of multi-electrode arrays using laparotomy can be used to obtain high-quality recordings, but are invasive and typically only conducted under anaesthesia, which can change gastric electrical activity[12,16]. Gastric mucosal recordings have been shown to exhibit comparable quality to serosal

recordings, enabling less invasive measurements, but electrodes are usually tethered endoscopically for acute measurements[17] or require nasally clipped leads, which are passed through the oesophagus to an external reader unit for awake recordings[18,19]. Recently, advances in electrogastrography signal processing have been made using artefact rejection algorithms[20], but there remains a need for devices that can record high-quality electrophysiology data from the ENS across the GI tract without any limitations to a subject's motion and comfort.

Ingestible electronic sensors offer a non-invasive method to monitor physiological signals[21,22]. They can be orally delivered and measure relevant information, such as core temperature, pressure, GI metabolites and gas concentration[21–24]. Ingestible devices also cause minimal disruption to the biology of the GI tract, as their placement does not require surgery or cause any damage to GI tissue. In this Article, we report an ingestible device for studying GI electrophysiology. The system, which is termed multimodal electrophysiology via ingestible, gastric, untethered tracking (MiGUT), contains encapsulated electronics and a battery (Fig. 1a,c), as well as a sensing electrode ribbon stored in a rolled configuration (Fig. 1d,e). Following delivery, the electrodes unroll in the stomach to make contact with the mucosa (Fig. 1b) and the device records biopotential signals, which are subsequently transmitted wirelessly to an external receiver several metres away. The location of the MiGUT device when placed in the stomach enables detection of electrical activity in the vital organs within close proximity. We show that this device can record high-quality biopotential signals, including the gastric slow wave, respiration rate and electrocardiogram, as well as putative signals related to the migrating myoelectric complex in a large animal model. We also show that the device can be transiently fixed to the gastric mucosa using endoscopic clips to measure and wirelessly transmit signals from the gastric slow wave during feeding, sleeping and ambulation over multiple days.

Device design and characterization

The MiGUT system shown in Fig. 2a consists of an electronics module and flexible measurement electrodes. The electronics are housed in a 9 × 12 × 26 mm (ref. 3) 3D-printed case (Fig. 2b), which was designed to be comparable to FDA cleared products such as capsule endoscopy systems (for example, Medtronic PillCam, ⌀11 × 26 mm; ⌀, diameter)[21] to facilitate future clinical translation. The entire body of the case and opening for measurement electrodes is sealed with ~0.5 mm of UV cure epoxy, covering all openings to ensure protection of the electronics environment from the gastric environment. The 3D-printed case, UV cure epoxy, polyamide electrode ribbon and gold electrodes were all selected from known biocompatible materials (Supplementary Table 1). In vitro testing indicates that electronics sealed in this manner can be maintained in simulated gastric fluid at 37 °C (pH = 2, n = 4; Methods) and wirelessly communicate for at least 4 days. Mechanical testing of the case body indicates that the force required to fracture the case (~250 N cm^{-2}) is substantially higher than that generated by the stomach (~4 N cm^{-2})[25], indicating that the device has mechanical robustness in the stomach (Supplementary Fig. 1).

Biopotentials are measured using an eight-channel, 16-bit analogue-to-digital converter (ADC) and are wirelessly transmitted to a base station using a microcontroller with integrated 915 MHz transceiver (Fig. 2c). The current consumption of the device depends on the sampling frequency, providing flexibility in balancing experiment length and signal fidelity. Duty cycling (Methods) between measurement and low power sleep mode enables experiments to be conducted over a number of days (Fig. 2d). With a panel antenna approximately 1–4 m (Methods) from the device in a freely moving swine (97 kg), an external 915 MHz transceiver was found to reliably receive over 99% of the data from the MiGUT system at approximately −70 dBm in a full stomach and during multiple behaviours (Fig. 2e).

A flat flexible cable connector on the electronics module enables a range of flexible electrode designs that can be used with the system,

such as custom designed electrodes fabricated using flexible printed circuit board (PCB) manufacturing methods (Supplementary Fig. 2 and Methods). In particular, a polyimide ribbon (total thickness 75 μm and 25 cm in length) containing eight gold recording electrodes and one reference electrode (double-sided, ⌀5 mm and ⌀8 mm, respectively) was developed specifically to span the greater curvature of the stomach and conform to the mucosa facilitating gastric recordings. The thickness of the polyimide ribbon was selected to (1) facilitate unrolling of the ribbon due to the inbuilt elasticity of the polyimide and copper and (2) enable the electrode ribbon to survive mechanical forces generated during entry of food into the stomach and churning as digestion occurs, while offering sufficient flexibility to conform to stomach mucosa. The double-sided electrodes ensure that the electrode can maintain contact with the gastric mucosa independent of ribbon orientation. The electrode is assembled in a rolled configuration secured with water soluble adhesive around a circular roller (Methods and Fig. 1d,e).

MiGUT safety and delivery

A potential safety concern of the MiGUT device is its long, linear structure once deployed. A review of literature indicates that linear devices such as the commercial EnteroTracker, containing a capsule and 90 cm nylon thread used for oesophageal string tests, have been safely demonstrated on human patients[25,26]. As the total length of the MiGUT capsule and ribbon is less than one third of the EnteroTracker, approximately 28 cm, this form factor was considered sufficiently safe for preliminary animal experiments.

Following delivery into the animal, MiGUT comes into contact with gastric fluid upon oral delivery to the stomach; the electrode unrolls due to inbuilt strain in the rolled ribbon along with the mechanical motion of the stomach (Supplementary Video 1). Preliminary safety of the MiGUT system was confirmed in passage studies showing that following delivery to the porcine stomach, the combined electronics and electrode ribbon system passes out of the animal by day 5 (n = 3, Supplementary Fig. 3). Reports in literature indicate that purely soft objects have a higher chance of being retained rather than passed in the gastrointestinal tract[26]. Retention was not observed in freely delivered MiGUT devices, which we attribute to the presence of the solid capsule body enabling the device to be propelled forward by peristalsis, in a manner similar to the structure of the capsule in the EnteroTracker system. Retrieval of devices after passage (Supplementary Fig. 3) shows that the ribbon is crumpled near the capsule, suggesting that the ribbon collapses over time around the capsule due to the forces of the GI, which facilitates device passage.

For longer experiments or measurements >24 h, the device can be clipped to the mucosa (Supplementary Fig. 4, n = 6), to allow for both device retention and stable long-term electrode contact in a manner similar to that reported in literature[27] supporting evaluation during solid food ingestion. Additionally, a suture loop can be attached to the MiGUT device to facilitate endoscopic manipulation and/or retrieval as necessary (Supplementary Video 2).

To demonstrate the recording capabilities of the MiGUT system in an in vivo porcine model, we designed a set of experiments to (1) record and assess signal components in anaesthetized animals, (2) validate the measurements using existing technologies, (3) assess inducted gastric electrophysiology changes with introduction of a gastric motility modulating compound in anaesthetized animals and (4) demonstrate recording in fully awake and ambulating animals.

Multimodal measurements in anaesthetized animals

In an anaesthetized Yorkshire pig, the device was delivered into the stomach and the electrode is shown to unroll and conform to the gastric mucosa along the greater curvature of the stomach (Fig. 3a). The reference electrode was localized near the stomach corpus (schematic in Supplementary Fig. 5a). One and a half hours of recorded data in
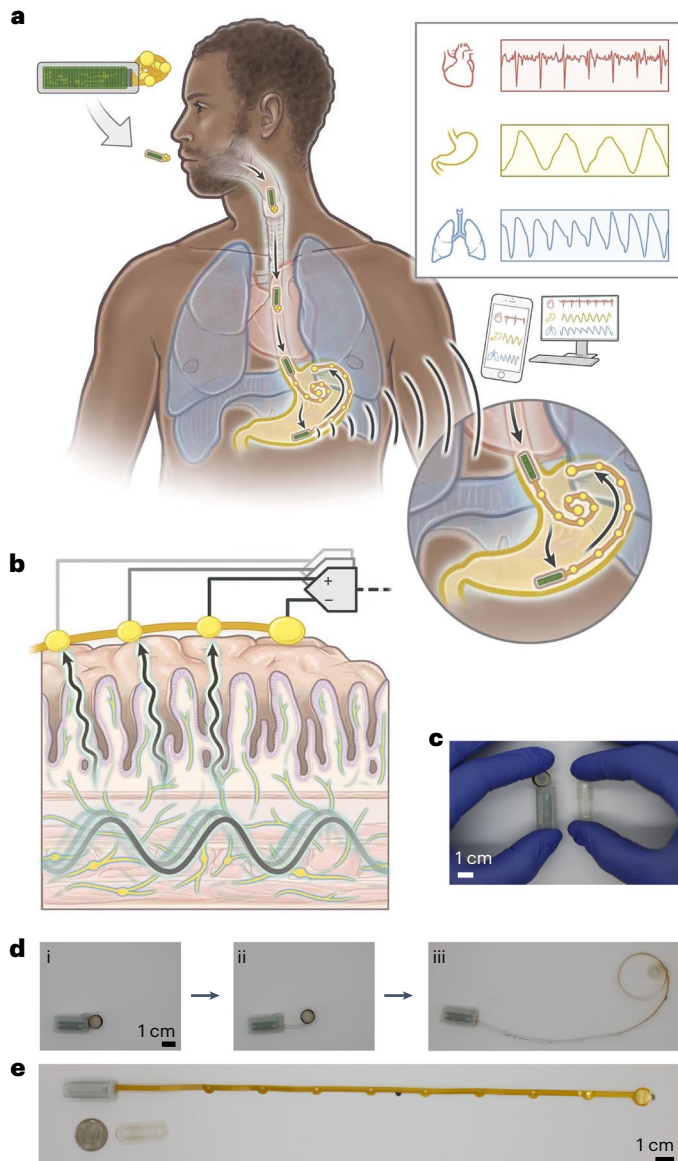
Fig. 1 | MiGUT device overview. a, Schematic representation of the MiGUT device containing electronics housed in an ingestible capsule with linear recording electrodes stored in a rolled configuration. Following ingestion, the electrodes unroll, come into contact with the mucosa and record gastric biopotentials, which can be wirelessly transmitted to an external receiver. The recorded data can be processed to extract heart rate, gastric slow wave and respiration rate. **b**, Schematic representation of electrodes deployed against the gastric mucosal surface. **c**, Size of MiGUT device in comparison to a 000 gelatin capsule. **d**, Unrolling of MiGUT electrodes due to strain of polyimide ribbon following wetting of water-soluble adhesive, showing the initial position (i), initiation of deployment (ii) and unrolling of electrodes (iii). **e**, Full extent of MiGUT device, total length of 25 cm. Dime and 000 gelatin capsules for scale.

this experiment (at 62.5 samples per second) was used to generate a heat map of electrical activity versus time for each channel (Fig. 3b(i)). Initial electrical activity seen in all channels following device placement (time, $t = 0$ to 500 s) is most likely due to mechanical stimulation as a consequence of endoscopic visualization following device deployment. Channels near the pylorus (Fig. 3b(ii), channels 0–2) measured large amplitude, prolonged waveforms with periods of about 500 s with approximately six total cycles. Additionally, observation of a representative 200 s window (Fig. 3c) in a single channel shows a waveform containing a superposition of several periodic signals. Band-pass filtering in the following windows reveals several distinct high-quality

signals of interest, ordered in power contribution to the raw signal: (1) 0.01 to 0.25 Hz: a periodic signal with frequency of approximately three cycles per minute, (2) 0.25 to 5 Hz: a periodic signal with dominant frequency around 26 cycles per minute and (3) over 5 Hz: a series of repeating spikes with a frequency of approximately 90 cycles per minute. These signals were also observed in separate experiments using the MiGUT system in different animals ($n = 9$, Supplementary Table 2 and Supplementary Fig. 6). Examination of a subset of channels in frequency range (1) shows similar waveforms with a propagation speed of ~3.3 cm s^{-1}, assuming linear electrode position, whereas no such propagation is observed in the contributions of frequency ranges (2) and (3) (Supplementary Fig. 7). Additionally, in a separate experiment, euthanization of the animal during MiGUT measurements, using a barbiturate cocktail, resulted in a cessation of all waveforms (Fig. 3d).

Due to the signal cessation following euthanization, we assess that all these signals in the various frequency windows discussed above are of physiologic origin. The observed waveforms with periods of approximately 500 s have not been previously reported in the literature in gastric mucosal or serosal electrophysiology measurements. We attribute this to a focus of previous studies on the gastric slow wave signal and consequent use of filtering, which would remove such low 'baseline fluctuations' (Supplementary Table 3) that we observe with the MiGUT system. The migrating motor complex (MMC) is known to exhibit electrical activity in the pyloric antrum and has a timescale of 90–120 min. The duration of measured signals may correspond to processes at an intermediate timescale between the gastric slow wave and the MMC, or are associated with an MMC phase or activity.

The 3 cycle per min signal is within the range expected for the gastric slow wave generated by interstitial cells of Cajal, and the shape of the waveform agrees qualitatively with that reported from nasal-clipped gastric mucosal signals and has a propagation speed on the same order of magnitude as that reported in literature for porcine experiments[18,19]. Moreover, we would expect this to be the dominant signal in the gastric environment in phases where the slow wave is active. The waveform with frequency of 26 cycles per min agrees well with the measured respiration rate observed on the vital signs monitor. In addition, the waveform shape agrees with transesophageal diaphragmatic electromyographic measurements conducted using catheter placed electrodes in the oesophagus[28,29]. Finally, the periodic spikes have a frequency of ~90 per min, which agrees well with the measured heart rate via the vital monitor and are similar in waveform to an electrocardiogram (EKG) measurement. The MiGUT experimental configuration of reference electrode and electrode ribbon spanning the interior of the stomach is similar to placement of cutaneous electrodes for a standard EKG measurement. Further analysis also shows that an EKG signal appears in all channels with the largest amplitude seen in channel 0, corresponding to the channel farthest from the reference electrode (Supplementary Fig. 8a), and the respiration signal appears in all channels, where amplitude variations between the individual channels are most likely due to the relative location of the measurement and reference electrodes and the diaphragm (Supplementary Fig. 8b). The amplitude of both the EKG and respiration signals remains stable throughout the measurement, suggesting that mucosal contact remains reliable for the measurement electrodes (Supplementary Fig. 8c,d). A separate porcine experiment with a MiGUT device confirms that measured heart rate agrees with measured changes in pulse rate on an external vital signs monitor (Supplementary Fig. 8e). We believe that observed biopotentials corresponding to the respiration rate and heart rate can be measured through electrodes in the stomach due to the close proximity of the stomach to vital organs, including the diaphragm and heart (Fig. 1a). Variability in the detected amplitudes in these frequency windows (Supplementary Table 2) can be attributed to variations in activity of the stomach, device placement and location of the reference electrode relative to the organ locations.
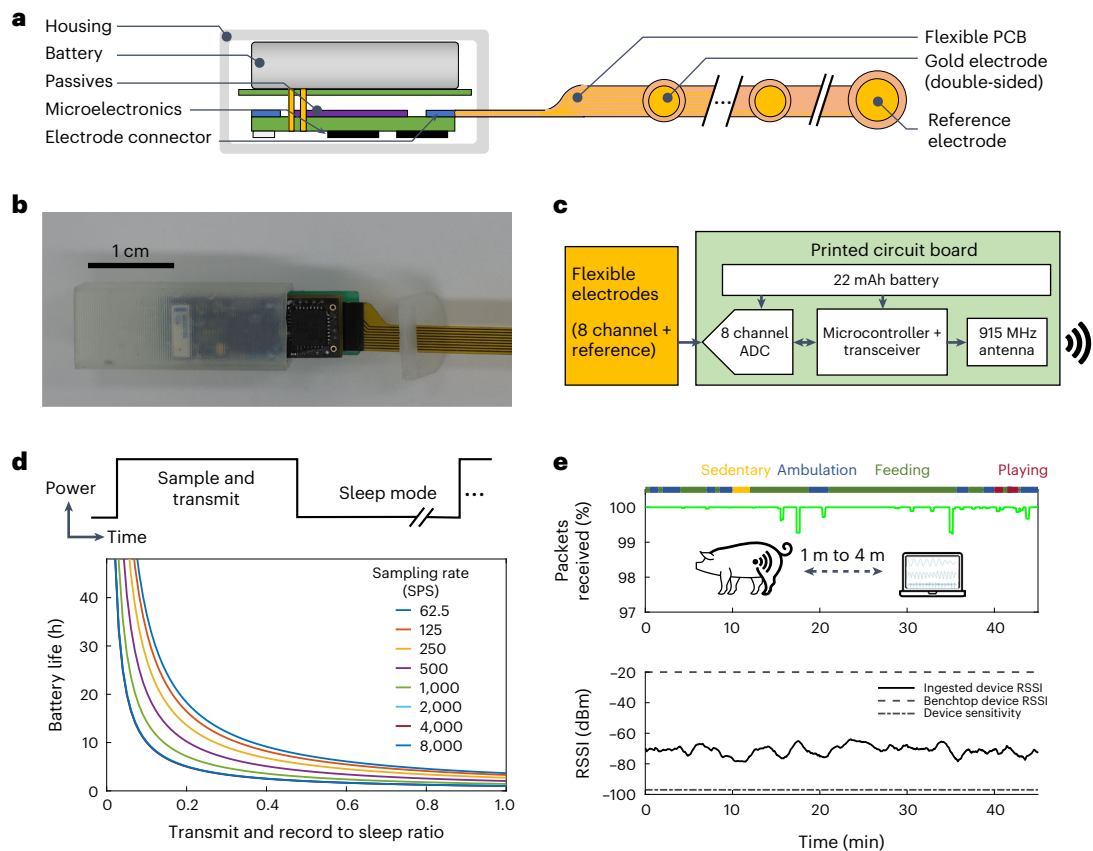
Fig. 2 | Design and in vivo evaluation of MiGUT system for multi-day, high-quality recordings. a, Schematic of device cross-section. **b**, Optical image of device components and assembly. **c**, Block diagram of electronics. **d**, Battery life of a system configured with different duty cycle ratios and sampling rates. A ratio of 1 indicates the battery life during continuous recording with no device sleep. **e**, Packets received and communication strength during different activities in a 97 kg, freely moving animal. RSSI, received signal strength indicator.

Validation of MiGUT measurements with existing technologies

To compare the recording quality of the non-invasive MiGUT system with other methods, we designed an experiment to conduct simultaneous recordings using the MiGUT device, along with serosal and cutaneous electrodes. MiGUT was orally delivered to an anaesthetized animal, following which two commercial Shimmer electromyography (EMG) systems (Shimmer A and Shimmer B) were placed on the exterior of the animal (Fig. 4a and Methods). Shimmer A, with an external cutaneous reference electrode (C-REF), was connected to electrodes on the skin surface for cutaneous recording and electrodes placed against the serosa via laparotomy, to replicate methods of gastric slow wave recording in the literature. Shimmer B, with an abdominal cavity reference electrode (A-REF), was connected to a serosal electrode. Simultaneous recordings from all devices yielded (1) small peaks at 3.1 cycles per min in the cutaneous channel, (2) no noticeable slow wave in the serosal (A-REF) channel, (3) a 3.1 cycles per min signal in the serosal (C-REF) channel and (4) an ~3.1 cycles per min signal in representative MiGUT channels (Fig. 4b). Furthermore, the cutaneous, serosal (C-REF) and MiGUT recordings show clear temporal agreement and spectrum analysis of the serosal, external and MiGUT recordings (Fig. 4c) with high peak frequencies and higher order peaks correlating to slow wave (3.1 cycles per min), respiration (18 cycles per min), EKG (85 cycles per min).

These simultaneous experiments show that MiGUT can achieve recording results comparable to surgically placed serosal electrodes that utilize an external reference electrode, supporting previous literature indicating that mucosal recordings are a viable strategy for accessing the gastric slow wave[17,18,29]. Differences in waveform shape can be attributed to variations in electrode placement location on the mucosal and serosal surface and the relative position of the electrodes. Interestingly, the data also show the importance of reference selection for recording of the gastric slow wave, as serosal electrodes placed with an internal reference could not measure the gastric slow wave, possibly due to noise from other organs in the abdominal cavity. Finally, the cutaneous measurements show smaller peaks, possibly due to tissue attenuation, which are otherwise in agreement with the frequency of the serosal and mucosal recordings, emphasizing that all methods are recording the same fundamental phenomenon of the gastric slow wave generated by the pacemaker potentials of the interstitial cells of Cajal and validating the functionality of the MiGUT device.

MiGUT measurements following prokinetic agent delivery

Motivated by the capability of the MiGUT system to detect gastric slow wave activity, we designed an experiment to test if the changes or modulations in gastric motility could also be detected. The MiGUT system was again placed in the porcine stomach of an anaesthetized animal; following baseline recording, azithromycin, a known prokinetic that activates motilin receptors[30] was intravenously delivered (1 mg kg^{-1} total dose) via ear catheter over the course of 5 min (Fig. 4d(i)). In five of the eight recording channels, a noticeable increase in power was observed over the following 25 min in the slow wave frequency range (Fig. 4d(ii) and Supplementary Fig. 9) in comparison to the 25 min before azithromycin dosing. In contrast, no meaningful change in power was observed in the EKG or respiratory frequency windows. Replicates of this experiment produced similar increases in the slow wave power (n = 4 total; Supplementary Fig. 10).
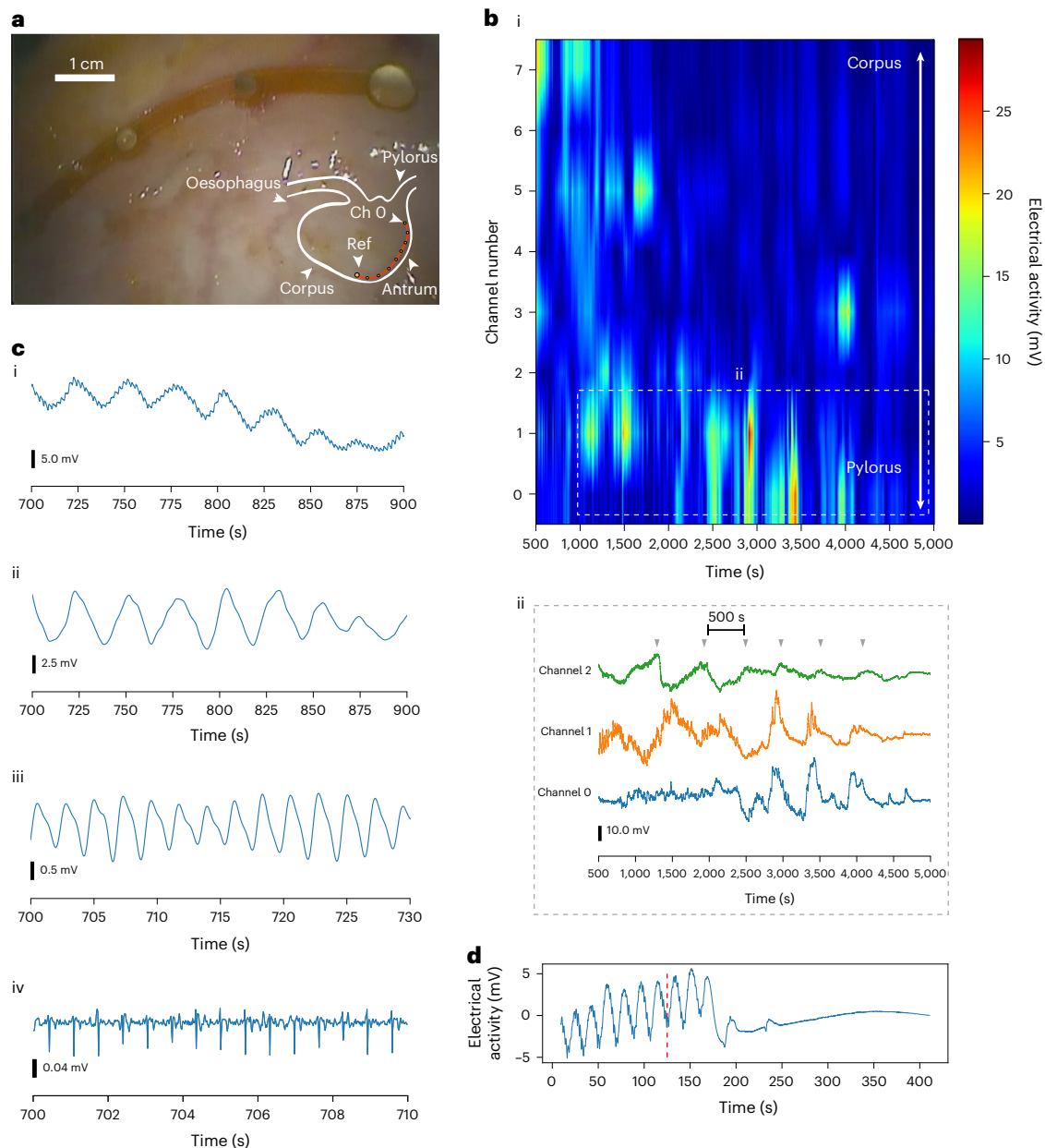
Fig. 3 | Acute recordings in an anaesthetized animal using MiGUT device.
a, Endoscopic image of MiGUT electrodes deployed against the gastric mucosa. Sensing electrodes ($\varnothing$5 mm) are distinguished from the reference (ref) electrode ($\varnothing$8 mm) by size. Inset: schematic of electrode and ref configuration. Channel (Ch) 0 was near the pylorus and the capsule body; channel 7 and ref were near the corpus. **b**, Recording in an anaesthetized animal showing heat map of electrical activity (0.0005 Hz to 15 Hz band-pass filter) over the course of ~1.5 h (i); voltage versus time of channels 0, 1 and 2 clear the pylorus, showing large waves with

a period of approximately 500 s putatively related to MMC activities (ii). Grey triangles indicate waves in channel 2. **c**, Representative single recording channel, sampling rate of 62.5 s^{-1}, showing raw collected data, 200 s (i), 'slow wave' band from 0.01 to 0.25 Hz, 200 s (ii), 'respiration' band from 0.25 to 5 Hz, 30 s (iii), 'EKG spikes' band from 5+ Hz (iv). Third-order Butterworth filters were used to extract all frequency bands. **d**, Cessation of electrical activities in a channel following animal euthanasia via barbiturate cocktail (delivery time indicated by dashed red line).

We attribute the observed increase in power of the slow wave to the alterations in gastric motility induced from the azithromycin delivery. The power in EKG and respiration windows remains constant, indicating electrode contact remains stable following azithromycin delivery (Fig. 4d(ii) and Supplementary Fig. 10). Of additional interest is the noted heterogeneity of the measured response in the different channels, which suggests that azithromycin, in addition to induction of increased slow wave activity, may also affect the spatial synchronization of the slow wave conduction along different parts of the GI tract. Qualitatively, this may also be consistent with commonly reported side effects of nausea, indigestion and vomiting following azithromycin administration[31], possibly as a consequence of desynchronization of the gastric slow wave.

MiGUT measurements in a freely moving large animal

Following experiments of the MiGUT system in anaesthetized animals, we wanted to further demonstrate the potential of the system for monitoring gastric electrophysiology in freely moving and feeding animals. MiGUT was delivered to the stomach of an anaesthetized swine and secured using endoscopic clips (endoscopic imaging in Supplementary Fig. 4 and schematic in Supplementary Fig. 5b). The animal was allowed to recover in its usual housing and after 1 h, timed data recording and transmission was then initiated from the MiGUT system for 3.5 h. Activity in the slow wave frequency window could be measured as the animal went through stages of feeding, ambulation and napping (Fig. 5a). Slow
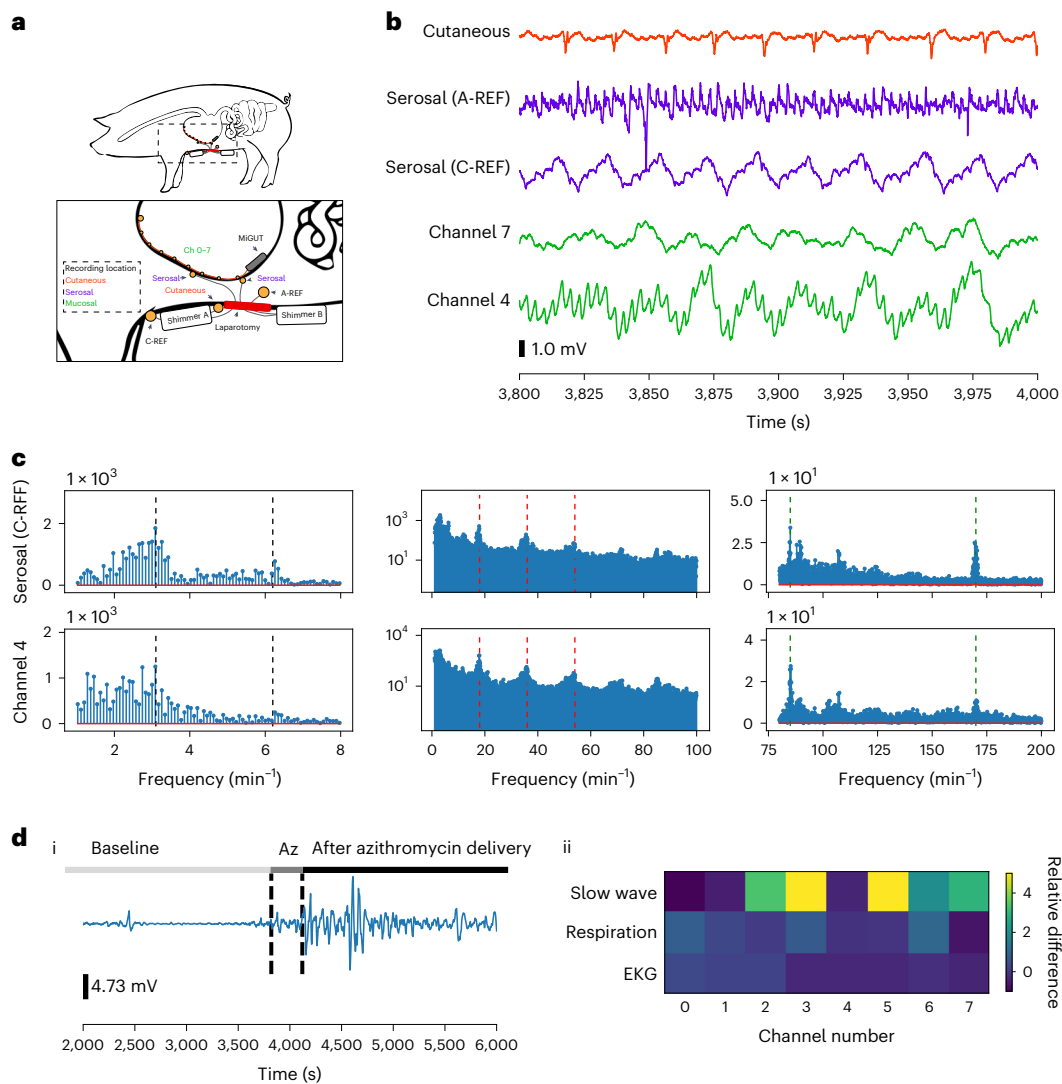
Fig. 4 | Validation of MiGUT measurements. a, Schematic representation of simultaneous recording using MiGUT system delivered orally, Shimmer3 commercial system (Shimmer A) with cutaneous and serosal electrodes and an external cutaneous reference away from the stomach, and another Shimmer3 (Shimmer B) with serosal electrodes and internal abdominal reference. Serosal electrodes and abdominal reference were placed following laparotomy. **b**, Data from simultaneous recording experiment showing frequency agreement between cutaneous, serosal/C-REF and two representative MiGUT channels. Serosal/A-REF recordings did not yield gastric slow wave recording, showing the importance of reference electrode position for obtaining high-quality signals. **c**, FFT comparison of serosal electrodes and a MiGUT recording channel at

a range of frequencies with dotted lines indicating dominant frequency and higher order peaks for slow wave (black, 3.1 cycles per min), respiration (red, 18 cycles per min) and EKG (green, 85 cycles per min) frequencies. **d**, Representative channel showing electrical activity before and following azithromycin delivery (0.01–0.25 Hz band-pass filter) in an anaesthetized animal (i). Heat map showing relative differences in signal power before and after azithromycin delivery in slow wave (0.01–0.25 Hz), respiration (0.25–5 Hz) and EKG (5+ Hz) frequency windows (ii). Relative difference was calculated by (initial power − final power)/(initial power) in 25 min windows before and following azithromycin delivery.

wave frequencies in all channels were between 3.5 and 4 cycles per min throughout the period of measurement (Fig. 5b and Supplementary Fig. 11). The amplitude of the slow waves varied depending on the animal's activities, showing 3–6 times higher slow wave amplitudes during feeding than during sleep or ambulation (Fig. 5c) as noted in representative data segments in a single representative channel.

The slow wave amplitudes recorded during animal ambulation and feeding were in the range of 5 mV to 27 mV (Supplementary Table 4), which are considerably higher than that observed in our anaesthetized measurements (0.5–4 mV, Fig. 3c and Supplementary Table 2), as well as those of cutaneous measurements (~50–200 μV) reported in literature[20]. The observed difference in amplitudes suggests anaesthesia suppresses gastric electrical activity. Additionally of interest, there appear to be minimal mechanical artefacts observed during animal ambulation, suggesting MiGUT can stably measure the gastric slow

wave during periods of heightened activities. The distinct increase in amplitude of slow wave activity during feeding and frequency stability of the slow wave agrees well with cutaneous wearable electrogastrogram devices[32]. Following feeding, the slow wave can still be stably measured, indicating that presence of food in the stomach does not inhibit device recordings. Finally, during these freely moving experiments, long period putatively MMC-related fluctuations were again observed in a subset of the channels, which may be of interest for future investigations (Supplementary Fig. 12).

Multi-day measurements were then taken in subsequent experiments to demonstrate the robust, long-term recording capabilities of MiGUT. In a first set of experiments, MiGUT was configured to record for 45 min (at 62.5 samples per second) separated by approximately 22 h of device sleep time and placed in a porcine subject in the same manner as the above ambulatory measurements. The frequency
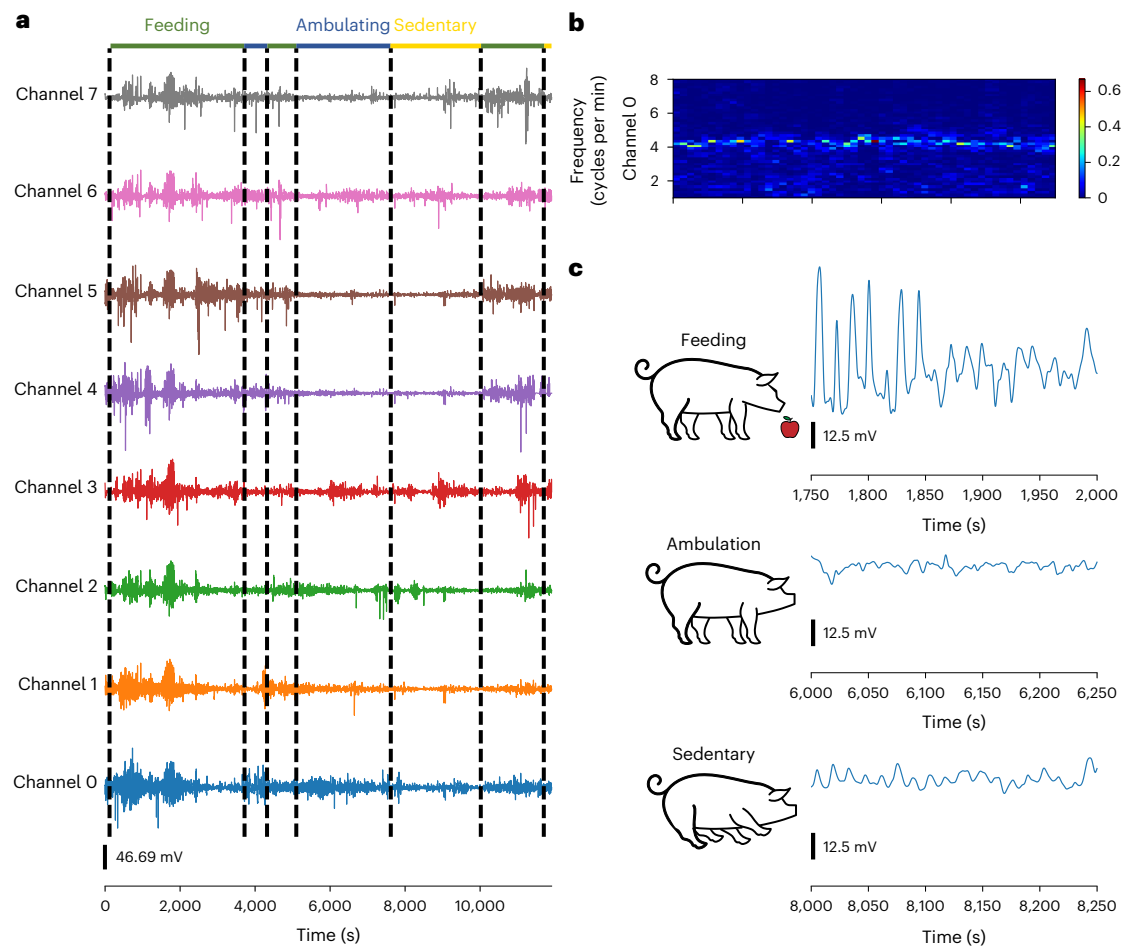
Fig. 5 | High-resolution measurements in an ambulating animal using MiGUT device. a, Eight-channel recording for 3.5 h from a MiGUT device secured in the porcine stomach (0.01–0.25 Hz band-pass filter) of a freely moving animal during feeding, ambulation and napping activities. **b**, Normalized power of frequencies versus time in the window of 1 to 8 cycles per min, showing a stable slow wave signal of approximately 4 cycles per min throughout animal activities. **c**, Representative segments of gastric electrical activity from channel 7 shown in **b** during feeding, ambulation and sleeping.

response from representative windows shows the slow wave can be detected on all three days, though it is less prevalent and of a slower frequency on day one when the animal was fasted (Fig. 6a) which is consistent with literature[32]. On day two after placement, the slow wave is still seen in all channels (Fig. 6b) along with increases in amplitude by ~3 times upon anticipation of (t = 1,297 s) and throughout (t = 1,415 s) feeding as previously discussed. This demonstrates the robustness of MiGUT to measure the slow wave after four meals were ingested, with no distortion seen once the meal was finished.

In a second set of experiments, MiGUT was configured to record at 30 samples per min (Methods), enabling ~40 h of continuous recording. The slow wave potential can be clearly seen, varying in amplitude and frequency over the course of the day (Fig. 6c and Supplementary Fig. 13). Following both of these extended experiments, the MiGUT device was retrieved, and no moisture ingression was observed on the interior of the capsule; the battery of the system could be recharged for reuse of the device (Methods).

Recording of the gastric slow wave for multiple days using MiGUT indicates the robustness and stability of the device design and placement. Future work could utilize this capability to gather sufficiently large data sets of gastric electrophysiology, which coupled with animal behaviour data and development of a data processing pipeline can be used to understand changes of gastric electrical activity as it relates to circadian rhythms and/or perturbations due to changes in diet or to pharmacological intervention.

Conclusions

Our ingestible MiGUT system is capable of recording high-quality electrical signals from the gastric environment, including the gastric slow wave, respiration rate and heart rate. It can also record long period waves, which may be associated with processes related to the migrating myoelectric complex. MiGUT can be used to monitor vital organs without requiring devices to be worn or implanted on the skin surface, which could be detached during subject activity. Additionally, while wearable commercial sensors that can detect respiration and EKG are readily available[33], wearable systems for monitoring the gastric slow wave typically require large surface arrays spanning most of the abdomen[32,34] and have noticeably reduced sensitivity in patients which have higher body mass indexes[35]. Moreover, our system can distinguish medication-induced motility changes and measure high-quality mucosal gastric slow waves during animal feeding and ambulation absent any tethering or wearable system. These results illustrate the potential for long-term study of gastric electrophysiology and a strategy to obtain high-quality recordings without restriction to subject movement, meals or day-to-day life.

Integrating other advances from the field of ingestible devices and neuro implants could address current limitations in the MiGUT system. For example, self-anchoring and resident capabilities[36,37] and wireless charging[38,39] could be incorporated into the system, and the channel count could be increased via multiplexing and onboard data filtering and processing. Moreover, there is potential for integration
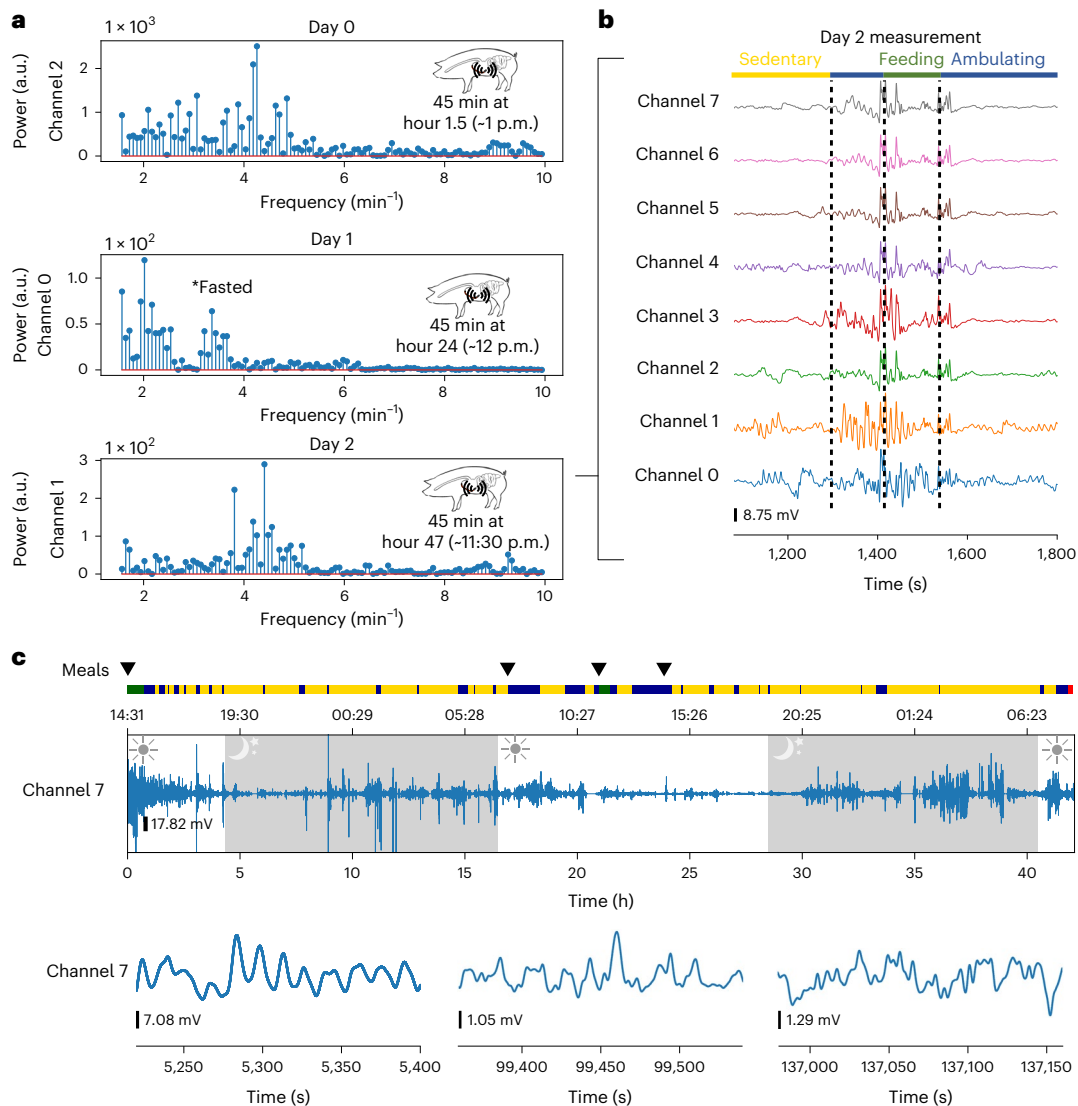
Fig. 6 | Multi-day measurements in an ambulating animal using MiGUT device. a, Dominant frequency response of representative windows after feeding (days 0 and 2) and when fasted (day 1). Recordings lasted 45 min each day separated by approximately 22 h of low power sleep mode. **b**, Measurements (0.01–0.25 Hz band-pass filter) taken from day 2 during different behaviours as annotated. **c**, Continuous multi-day measurement (0.01–0.25 Hz band-pass filter) with behaviours labelled as in **b**. Representative segments are shown (see additional channels in Supplementary Fig. 13).

with mucoadhesive and tissue-adhesive systems[40] or mechanically anchoring electrodes[36] to further enhance signal fidelity by ensuring tight contact between electrodes and the gastric mucosa. Integration with electrical stimulation systems[41] could enable development of novel closed-loop electroceuticals which reside in the GI tract. While passage studies in this work show that the MiGUT device can safely pass through the GI tract, additional safety characterization, as well as integration of degradable materials[42] into the electrode ribbon structure from developments in flexible electronics, could further enhance device safety before clinical translation. The recording ribbon could be further enhanced by decreasing film thickness to improve its capability to conform to the mucosal surface while maintaining its unrolling capability via integration of a sacrificial elastic backing. Self-orienting systems could also be considered to enable autonomous localization of the device in particular areas of the stomach[36,43].

With these developments, the system could be used to study hunger, satiety and circadian rhythms in the context of chronic GI disorders and could thus be used to understand fundamental changes in electrical signalling that occur with the onset of diseases such as gastroparesis or functional dyspepsia. The combination of ingestible electronics

and GI electrophysiology offers considerable potential for convenient at-home monitoring and could be used in the future to study gut–brain axis dysfunction for those with neurological and other disorders.

Methods
MiGUT electrodes

Three flexible PCB electrodes were developed for use in experiments with MiGUT (Supplementary Fig. 2). All were manufactured on 75-μm-thick polyimide with gold plated 0.5 oz copper traces and a 0.5-mm-pitch flat flexible connector (FFC) compatible interface on one end. The 'large' electrode used double-sided, 5-mm-diameter measurement electrodes with a 29.44 mm pitch, followed by an 8 mm reference electrode at the furthest end. Another configuration was also manufactured with the reference electrode closest to the FFC interface for convenient device placement. The 'medium' electrode was similar in size, but used 0.8-mm-diameter measurement electrodes with the same reference electrode configuration and spacing as the large electrode. The 'small' electrode used 0.8-mm-diameter electrodes with 3 mm pitch, followed by an 8 mm reference electrode. Unless otherwise specified, the large electrodes were used in the experiments

presented. To be compatible with Boston Scientific Resolution Clips for experiments with retention, 0.6-mm-diameter holes were added to the end of the electrode, with stiffener for mechanical support. This enabled ~10-mm-diameter loops of nitinol wire (NiTi Type 8, 0.025 mm, Fort Wayne Metals) to be attached to the electrode ribbon, which were secured to the mucosa using the Resolution Clips.

To validate there was no cross-talk between the channels, an impedance analyser (Sciospec ISX-3) was used to determine the electrode to electrode impedance. Representative two wire measurements between neighbouring electrodes and electrodes to the reference are shown in Supplementary Fig. 13. The high magnitude of the results indicates there is no cross-talk between electrodes, particularly at the low frequencies of interest.

MiGUT electronics

A six-layer PCB measuring 7×19.6 mm^2 was manufactured using 1.6 mm FR4 substrate, 1 oz copper traces and electroless nickel immersion gold pad finish. The FFCs (Molex, 5034801000), ADC (Texas Instruments, ADS131M08), microcontroller with integrated transceiver (Texas Instruments, CC1310), crystals (ECS, ECS-240-6-37B2-JTN-TR and Abracon, ABS04W-32.768KHZ-6-B2-T5) and power regulator (Onsemi, NCP170AMX330TBG) were then assembled with leadless solder. The schematic illustrating connections is shown in Supplementary Fig. 14. To provide power, a two-layer daughterboard measuring $7.16 \times 22.46 \times 0.51$ mm^3 securely mounts the 22 mAh Li-ion battery (Panasonic, CG-420) and is connected to the six-layer PCB with headers that are soldered in place. A Li-ion battery was chosen to support the continuous high current draw during wireless streaming of data. The MiGUT battery can be recharged and reused for multiple experiments (charging at 22 mA, 4.35 V, for ~2 h). The 915 MHz antenna (Ethertronics/AVX, M620720) is positioned on the outside face of the assembly to maximize radiation efficiency; recommended keep-out regions were maintained, and a pi matching network was implemented with datasheet recommended values. Impedance analysis using a vector network analyser (Keysight, E5080B) showed the antenna was not matched, but it still showed acceptable performance in vivo (Fig. 2e).

An off-the-shelf, eight-channel, simultaneous delta-sigma ADC is used to digitize biopotentials. All channels share the same reference, which are connected to the reference pin of the FFC header. The ADC can digitize all channels at sampling rates of 62.5 Hz to 8 kHz when provided with a 2.048 MHz clock, with 24 or 16 bit precision. For space efficiency, the clock signal is provided by the microcontroller at 2 MHz, and the desired sampling rates were confirmed to be maintained by injecting a signal at various frequencies and comparing the measured signal.

MiGUT configuration

An overview of the device configuration and data flow is presented in Supplementary Fig. 16. The Cortex-M3 microcontroller is programmed to first initialize the ADC for low power, 16-bit mode, at a programmed sampling rate and signal amplifier gain configuration. The microcontroller communicated with the ADC over a Serial Peripheral Interface at 4 MHz with the clock polarity low during idle and data sampled on the falling edge of the clock (mode 1). For the in vivo experiments presented, a sampling rate of 62.5 samples per second was selected for power efficiency, and a range of ±600 mV, ±300 mV or ±150 mV was selected, depending on the length of the experiment, to account for drift. Filters on the ADC to remove low frequency noise are available, but not used during these experiments due to the frequency band of the desired signals. To reduce power, the microcontroller only initializes critical modules and shuts down peripherals used during debugging. The device transmits confirmation that initialization was complete and then transitions to an ultra-low power mode for a programmed amount of time. Two programmable arrays allow for complete customizability in sequential lengths of sleep and number of samples taken before transitioning to the other state. Unless otherwise specified, for ambulation experiments, the

device is turned on immediately before placement, sleeps for 1.5 h, then records 168,750 samples (for 45 min, to capture long trends) and sleeps for 22.5 h (a 2% duty cycle ratio). During sampling, the ADC triggers an interrupt when new data is ready, which is then loaded into a buffer that transmits the data while simultaneously receiving new data. For low sampling rates, the device can automatically go into a lower power state after transmission while it is waiting for the next sample. The ADC data arriving at the microcontroller are packetized and wirelessly transmitted at 14 dBm Tx power using 500 kB s^{-1} symbol rate at 915 MHz with a deviation of 175 kHz and Rx filter bandwidth of 1,242 kHz. Data from all channels are transmitted with a packet number and checksum CRC for error correction as they arrive from the MiGUT device.

To evaluate the trade-off between data throughput and power consumption, the current consumption of the device is measured using the Nordic PPK under different device configurations. When configured to sample at 62.5 samples per second and stream the data continuously, the MiGUT system consumed an average of 6.28 mA with peaks at 21.5 mA. During sleep mode, the MiGUT system consumed 50 μA on average. The results when changing the sampling rate are shown in Fig. 2d.

For extended experiments, further power cycling was achieved by sleeping the ADC and MCU between sampling times. The MCU and ADC were configured to sleep for 1.8 s, followed by recording of eight samples from the ADC. The first three samples of the ADC were discarded due to transients from device wake-up and the remaining samples were transmitted externally and averaged in postprocessing to obtain an effective sampling rate of 1 sample per 2 seconds. In this configuration, the MiGUT system consumed an average of 0.5 mA with peaks of 21.5 mA during RF transmission.

Receiver board configuration

A Texas Instruments LAUNCHXL-CC1310 evaluation board with a panel antenna (TE Connectivity PAL902010-FNF) was connected to a laptop and used with Texas Instruments SmartRF Studio 7 (v.2.23.0) to save the data to a text file. While a benchtop receiver setup was used, commercially available USB dongles such as the Texas Instruments CC1111EMK868-915 enable data to be recorded to a mobile device.

Frequency response of MiGUT electronics

MiGUT was connected directly to a Tektronix AFG3102 function generator, and a 100 mV peak-to-peak sine wave was injected from frequencies spanning 100 μHz to 62.5 Hz. MiGUT was programmed with the same code used in the animals and wirelessly streamed the data to a receiver board described above. The measured signals were then compared to the input waveforms and manually aligned to correct for phase shift. The magnitudes were compared and shown in Supplementary Fig. 17.

MiGUT device assembly

The three-dimensional (3D) device case was fabricated using a Form-labs 2 3D printer (durable resin) in three pieces: the main capsule body and two press-fit case caps, one of which has a designed opening for the electrode ribbon to pass through. The PCB is placed into the printed case, the electrode ribbon is connected to the FCC connector, passed through the in the case cap and then both ends of the case closed using the printed caps. The entire capsule is then sealed with UV cure epoxy (Loctite 4305) using a UV lamp. The other end of the electrode ribbon is bound to a 3D-printed circular roller (9 mm diameter) using water soluble adhesive tape (SmartSolve) and the electrode is rolled up onto the roller and fixed against the case using the same water soluble tape. For endoscopic clipping experiments, nylon loops are passed to predesigned mounting points in the case, and a nitinol loop is passed through the via in the stiffened hole on the double-sided reference electrode. Only the recording ribbon and epoxy encapsulation are exposed to the gastric environment, all of which have been shown to be safe and used in prior ingestible and implantable devices, with details of their biocompatibility provided in Supplementary Table 1.

Simulated gastric fluid testing

MiGUT PCB boards were placed into their 3D-printed cases and sealed with Loctite 4305 UV cure epoxy, as discussed in the device assembly. Devices were placed in the containers of simulated gastric fluid (Sigma-Aldrich) on a shaker tray moving at 25 r.p.m. at 37 C as a simulation of the gastric environment. Electronics survival was validated by sending a message packet from the MiGUT board to an external receiver board every minute.

MiGUT capsule fracture test

MiGUT devices were assembled without the electronics and force tested using an Admet eXpert 5952. The capsule was positioned both vertically and horizontally, pressed between two plates. A linear sweep was then performed, measuring the force exerted on the capsule by position sampling at 100 Hz.

In vivo testing

All animal experiments were approved by and performed in accordance with the Committee on Animal Care at MIT. Yorkshire swine were obtained from the Cummings School of Veterinary Medicine at Tufts University for in vivo experiments. Pigs weighing approximately 60–100 kg were placed on a liquid diet for 24 h the day before the study and were fasted overnight before the study. For device placement, animals were anaesthetized using an intramuscular injection of midazolam 0.25 mg kg^{-1} and dexmedetomidine 0.03 mg kg^{-1}. Following sedation, animals were placed on thermal support and ophthalmic ointment was applied to both eyes. The animal was intubated and placed on isoflurane (2%) in oxygen and connected to a vital signs monitoring system. The MiGUT device was delivered orally into the stomach, using an orogastric tube and imaged using PENTAX EC-3870TLK (160 cm) to visualize the stomach with the animal in the left lateral position. Following delivery and endoscopic imaging, the stomach of the animal was deflated via use of the endoscope to ensure contact of the electrodes with the stomach.

Animal euthanasia study

For non-survival procedures, the animal was sedated with an intramuscular injection of Telazol (tiletamine/zolazepam) 5 mg kg^{-1} and xylazine 2 mg kg^{-1} and euthanized using Fatal Plus (sodium pentobarbital), 1 ml per 10 lbs. Heart rate and respiration rate were assessed via vitals monitor to ensure that the pig had been euthanized.

Gastric transit studies

For gastric transit studies, a device with the same form factor but enhanced X-ray contrast was used. The interior compartment of the MiGUT device was filled with stainless steel powder (Sigma-Aldrich) to a comparable weight of 3.5–4.0 g instead of housing the electronics to allow higher contrast under X-ray imaging (Supplementary Fig. 3). The device was delivered to the anaesthetized animal orally through an overtube and then endoscopically imaged to confirm unrolling in the stomach. All devices ($n = 3$) were radiographically confirmed as excreted by day 5 and were recovered in faeces. One device was observed to have a broken ribbon, which we assessed to have occurred following excretion, due to animal activity.

Simultaneous recording study

The animal was sedated with an intramuscular injection of Telazol (tiletamine/zolazepam) 5 mg kg^{-1} and xylazine 2 mg kg^{-1}. The animal was intubated and placed on isoflurane (2%) in oxygen and connected to a vital signs monitoring system. The MiGUT device was delivered in the above-described manner. Following MiGUT delivery, a midline laparotomy was conducted to enable placement of serosa electrodes (Gold, flexible PCB substrate, OSH Park), which were backed with saline soaked gauze as per literature[12]. Standard EMG/ECG electrodes were placed in the abdominal area near the stomach and used for cutaneous measurements. All serosal and cutaneous electrodes were connected to a Shimmer3 Recording system (Shimmer Sensing, Boston, USA), where the reference electrode was either a metallic clip on the interior of the abdomen (A-REF), or a standard EMG electrode placed away from the abdominal area (C-REF). Animal was euthanized using Fatal Plus (sodium pentobarbital), 1 ml per 10 lbs following measurements.

Azithromycin motility experiments measurements

For azithromycin experiments, following about 1 h of baseline recording in the anaesthetized animal, 1 mg kg^{-1} animal weight of 20 mg ml^{-1} Azithromycin (Sigma-Aldrich) solution (in PBS pH adjusted with HCl, Thermofischer) was delivered via ear catheter over the course of 5 min. Measurements were conducted for a minimum of 45 min following drug delivery. Power was calculated by summing the square of the voltage measurements in a 25 min time window. Difference in power p was calculated as $(p_{initial} - p_{final})/p_{initial}$.

Ambulating measurements

Electrodes were fixed to the mucosa (Supplementary Fig. 5b) following oral delivery using three resolution endoclips (Boston Scientific). Two endoclips were placed on the ends of the electronics capsule body and the third on a nitinol loop attached to the reference electrode. Following device delivery and clipping, the swine was allowed to recover for at least 1 h from anaesthesia, before ambulating MiGUT measurements. During recovery, the pig was closely monitored until extubation. The animals were returned to their pen and dexmedetomidine was reversed via intramuscularly injected, atipamezole, 0.1 mg kg^{-1}. During the recovery process, the animal was monitored until it was considered bright, alert and responsive. The external 915 MHz receiver was either placed on a wheeled cart outside of the animal pen or mounted on the ceiling of the pen, and animals were fed approximately 1–2 h following recovery. Device was confirmed to be retained in the stomach 48 h following clipping via endoscopic imaging.

Data analysis

Recorded data was parsed using custom code written in Python using pandas, numpy, matplotlib and scipy libraries. Signal processing was conducted using the scipy signals module, and graphical representations of data were generated using matplotlib. An outline of the pipeline is shown in Supplementary Fig. 16.

Reporting summary

Further information on research design is available in the Nature Portfolio Reporting Summary linked to this article.

Data availability

The data that supports the findings of this study are available at https://github.com/adamgierlach/MiGUT_data_repository.

Code availability

The code that supports the findings of this study is available at https://github.com/adamgierlach/MiGUT_data_repository.

References

1. Furness, J. B. The enteric nervous system and neurogastroenterology. *Nat. Rev. Gastroenterol. Hepatol.* **9**, 286–294 (2012).
2. Spencer, N. J. & Hu, H. Enteric nervous system: sensory transduction, neural circuits and gastrointestinal motility. *Nat. Rev. Gastroenterol. Hepatol.* **17**, 338–351 (2020).
3. Camilleri, M. et al. Gastroparesis. *Nat. Rev. Dis. Prim.* **4**, 41 (2018).
4. Grover, M., Farrugia, G. & Stanghellini, V. Gastroparesis: a turning point in understanding and treatment. *Gut* **68**, 2238–2250 (2019).
5. Mahadeva, S. Epidemiology of functional dyspepsia: a global perspective. *World J. Gastroenterol.* **12**, 2661 (2006).

6. Travagli, R. A., Browning, K. N. & Camilleri, M. Parkinson disease and the gut: new insights into pathogenesis and clinical relevance. *Nat. Rev. Gastroenterol. Hepatol.* **17**, 673–685 (2020).

7. Jones, J. D., Rahmani, E., Garcia, E. & Jacobs, J. P. Gastrointestinal symptoms are predictive of trajectories of cognitive functioning in de novo Parkinson's disease. *Parkinsonism Relat. Disord.* **72**, 7–12 (2020).

8. Warnecke, T., Schäfer, K.-H., Claus, I., Del Tredici, K. & Jost, W. H. Gastrointestinal involvement in Parkinson's disease: pathophysiology, diagnosis, and management. *npj Parkinsons Dis.* **8**, 31 (2022).

9. Hsiao, E. Y. Gastrointestinal issues in autism spectrum disorder. *Harv. Rev. Psychiatry* **22**, 104–111 (2014).

10. Saurman, V., Margolis, K. G. & Luna, R. A. Autism spectrum disorder as a brain-gut-microbiome axis disorder. *Dig. Dis. Sci.* **65**, 818–828 (2020).

11. Farajidavar, A. Bioelectronics for mapping gut activity. *Brain Res.* **1693**, 169–173 (2018).

12. O'Grady, G. et al. Methods for high-resolution electrical mapping in the gastrointestinal tract. *IEEE Rev. Biomed. Eng.* **12**, 287–302 (2019).

13. Keller, J. et al. Advances in the diagnosis and classification of gastric and intestinal motility disorders. *Nat. Rev. Gastroenterol. Hepatol.* **15**, 291–308 (2018).

14. Sanders, K. M., Koh, S. D. & Ward, S. M. Interstitial cells of Cajal as pacemakers in the gastrointestinal tract. *Annu. Rev. Physiol.* **68**, 307–343 (2006).

15. Alvarez, W. The electrogastrogram and what it shows. *J. Am. Med. Assoc.* **78**, 1116 (1922).

16. Lammers, W. J. E. P., Stephen, B., Arafat, K. & Manefield, G. W. High resolution electrical mapping in the gastrointestinal system: initial results. *Neurogastroenterol. Motil.* **8**, 207–216 (1996).

17. Angeli, T. R. et al. High-resolution electrical mapping of porcine gastric slow-wave propagation from the mucosal surface. *Neurogastroenterol. Motil.* **29**, e13010 (2017).

18. Paskaranandavadivel, N. et al. Ambulatory gastric mucosal slow wave recording for chronic experimental studies. In *39th Annual International Conference of the IEEE Engineering in Medicine and Biology Society (EMBC)* 755–758 (IEEE, 2017); https://doi.org/10.1109/EMBC.2017.8036934

19. Paskaranandavadivel, N. et al. Multi-day, multi-sensor ambulatory monitoring of gastric electrical activity. *Physiol. Meas.* **40**, 025011 (2019).

20. Gharibans, A. A. et al. Artifact rejection methodology enables continuous, noninvasive measurement of gastric myoelectric activity in ambulatory subjects. *Sci. Rep.* **8**, 5019 (2018).

21. Steiger, C. et al. Ingestible electronics for diagnostics and therapy. *Nat. Rev. Mater.* **4**, 83–98 (2019).

22. Yang, S.-Y. et al. Powering implantable and ingestible electronics. *Adv. Funct. Mater.* **31**, 2009289 (2021).

23. Kalantar-Zadeh, K. et al. A human pilot trial of ingestible electronic capsules capable of sensing different gases in the gut. *Nat. Electron.* **1**, 79–87 (2018).

24. De la Paz, E. et al. A self-powered ingestible wireless biosensing system for real-time in situ monitoring of gastrointestinal tract metabolites. *Nat. Commun.* **13**, 7405 (2022).

25. Koziolek, M. et al. Intragastric pH and pressure profiles after intake of the high-caloric, high-fat meal as used for food effect studies. *J. Control. Release* **220**, 71–78 (2015).

26. Sarker, S., Jones, R., Chow, G. & Terry, B. Design of a soft, self-uncoiling stent for extended retention of drug delivery in the small intestine. In *Proc. 2021 Design of Medical Devices Conference* V001T12A010 (ASME, 2021); https://doi.org/10.1115/DMD2021-1063

27. Schostek, S. et al. Pre-clinical study on a telemetric gastric sensor for recognition of acute upper gastrointestinal bleeding: the "HemoPill monitor". *Surg. Endosc.* **34**, 888–898 (2020).

28. Hutten, G. J., van Thuijl, H. F., van Bellegem, A. C. M., van Eykern, L. A. & van Aalderen, W. M. C. A literature review of the methodology of EMG recordings of the diaphragm. *J. Electromyogr. Kinesiol.* **20**, 185–190 (2010).

29. Lokin, J. L., Dulger, S., Glas, G. J. & Horn, J. Transesophageal versus surface electromyography of the diaphragm in ventilated subjects. *Respir. Care* **65**, 1309–1314 (2020).

30. Sanger, G. J. & Furness, J. B. Ghrelin and motilin receptors as drug targets for gastrointestinal disorders. *Nat. Rev. Gastroenterol. Hepatol.* **13**, 38–48 (2016).

31. Hopkins, S. Clinical toleration and safety of azithromycin. *Am. J. Med.* **91**, S40–S45 (1991).

32. Gharibans, A. A. et al. Gastric dysfunction in patients with chronic nausea and vomiting syndromes defined by a noninvasive gastric mapping device. *Sci. Transl. Med.* **14**, eabq3544 (2022).

33. Ray, T. R. et al. Bio-integrated wearable systems: a comprehensive review. *Chem. Rev.* **119**, 5461–5533 (2019).

34. Vujic, A. et al. Gut-brain computer interfacing (GBCI): wearable monitoring of gastric myoelectric activity. In *41st Annual International Conference of the IEEE Engineering in Medicine and Biology Society (EMBC)* 5886–5889 (IEEE, 2019); https://doi.org/10.1109/EMBC.2019.8856568

35. Obioha, C. et al. Effect of body mass index on the sensitivity of magnetogastrogram and electrogastrogram. *J. Gastroenterol. Hepatol. Res.* **2**, 513–519 (2013).

36. Abramson, A. et al. Ingestible transiently anchoring electronics for microstimulation and conductive signaling. *Sci. Adv.* **6**, eaaz0127 (2020).

37. Kong, Y. L. et al. 3D-printed gastric resident electronics. *Adv. Mater. Technol.* **4**, 1800490 (2019).

38. Abid, A. et al. Wireless power transfer to millimeter-sized gastrointestinal electronics validated in a swine model. *Sci. Rep.* **7**, 46745 (2017).

39. Javan-Khoshkholgh, A., Sassoon, J. C. & Farajidavar, A. A wireless rechargeable implantable system for monitoring and pacing the gut in small animals. In *2019 IEEE Biomedical Circuits and Systems Conference (BioCAS)* 1–4 (IEEE, 2019); https://doi.org/10.1109/BIOCAS.2019.8919125

40. Yuk, H., Wu, J. & Zhao, X. Hydrogel interfaces for merging humans and machines. *Nat. Rev. Mater.* **7**, 935–952 (2022).

41. Ramadi, K. B., Srinivasan, S. S. & Traverso, G. Electroceuticals in the gastrointestinal tract. *Trends Pharmacol. Sci.* **41**, 960–976 (2020).

42. Li, C. et al. Design of biodegradable, implantable devices towards clinical translation. *Nat. Rev. Mater.* **5**, 61–81 (2020).

43. Abramson, A. et al. An ingestible self-orienting system for oral delivery of macromolecules. *Science* **363**, 611–615 (2019).

Acknowledgements

Author contributions

S.S.Y., A.G., P.S., H.-W.H. and G.T. conceived and designed the research. S.S.Y., A.G., G.S., I.M., P.S. and S.-Y.Y. designed, tested and validated electronics. S.S.Y., A.G., P.S., S.-Y.Y., K.I., W.A.M.M., J.J. and A.H. performed animal experiments. S.S.Y., A.G., G.S. and I.M. wrote device firmware. S.S.Y. and A.G. wrote software to analyse data. S.S.Y., A.G., P.S., S.O. and G.T. interpreted results. S.S.Y., A.G., P.S., A.P.C. and G.T. wrote the paper. All authors reviewed and approved the paper.

Competing interests

Financial competing interests for G.T. that may be interpreted as related to the current paper include current and prior funding from Novo Nordisk, Hoffman La Roche, Oracle, Draper Laboratory, MIT Lincoln Laboratory, NIH (NIBIB and NCI), Bill and Melinda Gates Foundation, The Leona M. and Harry B. Helmsley Charitable Trust, Karl van Tassel (1925) Career Development Professor, MIT, the Defense Advanced Research Projects Agency, and the Advanced Research Projects Agency for Health (ARPA-H) as well as employment by the Massachusetts Institute of Technology and Brigham and Women's Hospital. Personal financial interests include equity/stock (Lyndra Therapeutics, Suono Bio, Vivtex, Celero Systems, Syntis Bio), board of directors member and/or consultant (Lyndra Therapeutics, Novo Nordisk, Suono Bio, Vivtex, Celero Systems, Syntis Bio) and royalties (past and potentially in the future) from licensed and/or optioned intellectual property (Lyndra Therapeutics, Novo Nordisk, Suono Bio, Vivtex, Celero Systems, Syntis Bio, Johns Hopkins, MIT, Mass General Brigham Innovation). Complete details of all relationships for profit and not-for-profit for G.T. can be found in Supplementary Information. The authors S.S.Y., A.G., G.S., S.-Y.Y. and G.T., with R. Langer, report a patent application (US Provisional Patent Application No. 63/589,401) describing the system reported in the paper. The other authors declare no competing interests.

Additional information

Supplementary information The online version contains supplementary material available at https://doi.org/10.1038/s41928-024-01160-w.

Correspondence and requests for materials should be addressed to Giovanni Traverso.

Peer review information *Nature Electronics* thanks Aydin Farajidavar, Bozhi Tian and the other, anonymous, reviewer(s) for their contribution to the peer review of this work.

Reprints and permissions information is available at www.nature.com/reprints.

nature portfolio

Corresponding author(s): Traverso

Last updated by author(s): Mar 30, 2023

Reporting Summary

Nature Portfolio wishes to improve the reproducibility of the work that we publish. This form provides structure for consistency and transparency in reporting. For further information on Nature Portfolio policies, see our Editorial Policies and the Editorial Policy Checklist.

Statistics

For all statistical analyses, confirm that the following items are present in the figure legend, table legend, main text, or Methods section.

n/a	Confirmed	
☐	☒	The exact sample size (*n*) for each experimental group/condition, given as a discrete number and unit of measurement
☐	☒	A statement on whether measurements were taken from distinct samples or whether the same sample was measured repeatedly
☒	☐	The statistical test(s) used AND whether they are one- or two-sided *Only common tests should be described solely by name; describe more complex techniques in the Methods section.*
☒	☐	A description of all covariates tested
☐	☒	A description of any assumptions or corrections, such as tests of normality and adjustment for multiple comparisons
☐	☒	A full description of the statistical parameters including central tendency (e.g. means) or other basic estimates (e.g. regression coefficient) AND variation (e.g. standard deviation) or associated estimates of uncertainty (e.g. confidence intervals)
☒	☐	For null hypothesis testing, the test statistic (e.g. *F*, *t*, *r*) with confidence intervals, effect sizes, degrees of freedom and *P* value noted *Give P values as exact values whenever suitable.*
☒	☐	For Bayesian analysis, information on the choice of priors and Markov chain Monte Carlo settings
☒	☐	For hierarchical and complex designs, identification of the appropriate level for tests and full reporting of outcomes
☒	☐	Estimates of effect sizes (e.g. Cohen's *d*, Pearson's *r*), indicating how they were calculated

Our web collection on statistics for biologists contains articles on many of the points above.

Software and code

Policy information about availability of computer code

Data collection	The MiGUT device contains a Texas Instruments CC1130 microcontroller which runs custom firmware written using code composer studio 11.1.0 from Texas Instruments, and collects and transmits data recorded using the Texas Instruments ADS131M08. We used SmartRF Studio 7 from Texas Instruments along with a receiver board to collect data transmitted wirelessly from the MiGUT device inside the stomach of the animal. Code written in Python was used to decode the collected packets into measured potentials. All custom code is available on reasonable request from the author.
Data analysis	Data was analyzed using Python 3 and plotted using the Python Matplotlib library or MATLAB. Code is available on reasonable request from the corresponding author.

For manuscripts utilizing custom algorithms or software that are central to the research but not yet described in published literature, software must be made available to editors and reviewers. We strongly encourage code deposition in a community repository (e.g. GitHub). See the Nature Portfolio guidelines for submitting code & software for further information.

Data

Policy information about availability of data

All manuscripts must include a data availability statement. This statement should provide the following information, where applicable:

- Accession codes, unique identifiers, or web links for publicly available datasets
- A description of any restrictions on data availability
- For clinical datasets or third party data, please ensure that the statement adheres to our policy

For experimental measured data, the manuscript provides analyzed data. Raw data is accessible by request.

Human research participants

Policy information about studies involving human research participants and Sex and Gender in Research.

Reporting on sex and gender	N/A
Population characteristics	N/A
Recruitment	N/A
Ethics oversight	N/A

Note that full information on the approval of the study protocol must also be provided in the manuscript.

Field-specific reporting

Please select the one below that is the best fit for your research. If you are not sure, read the appropriate sections before making your selection.

☒ Life sciences   ☐ Behavioural & social sciences   ☐ Ecological, evolutionary & environmental sciences

For a reference copy of the document with all sections, see nature.com/documents/nr-reporting-summary-flat.pdf

Life sciences study design

All studies must disclose on these points even when the disclosure is negative.

Sample size	Sample sizes were chosen based on preliminary experiments and prior work with ingestible electronics devices, to provide sufficient power for statistical comparison when needed.
Data exclusions	No data values were excluded in the analysis.
Replication	Each experiment presented in the paper was repeated in multiple animals with various number of replicates. The number of animal and replicates are presented in the text or figure.
Randomization	Randomization of animals was not applicable for our studies
Blinding	Blinding was not applicable for the studies as there was no control vs experimental group for testing of our device. All analysis was quantative, and conducted in the same manner over the varied experiments

Reporting for specific materials, systems and methods

We require information from authors about some types of materials, experimental systems and methods used in many studies. Here, indicate whether each material, system or method listed is relevant to your study. If you are not sure if a list item applies to your research, read the appropriate section before selecting a response.

Materials & experimental systems

n/a	Involved in the study
☒	☐ Antibodies
☒	☐ Eukaryotic cell lines
☒	☐ Palaeontology and archaeology
☐	☒ Animals and other organisms
☒	☐ Clinical data
☒	☐ Dual use research of concern

Methods

n/a	Involved in the study
☒	☐ ChIP-seq
☒	☐ Flow cytometry
☒	☐ MRI-based neuroimaging

Animals and other research organisms

Policy information about studies involving animals; ARRIVE guidelines recommended for reporting animal research, and Sex and Gender in Research

Laboratory animals	Female Yorkshire Swine aged 4-8 months (60-100kg)
Wild animals	NA
Reporting on sex	Female Yorkshire Swine
Field-collected samples	NA
Ethics oversight	This study is approved by MIT committee on Animal Care

Note that full information on the approval of the study protocol must also be provided in the manuscript.